第33卷 第9期 焊 接 学 报 Vol. 33 No. 9
2012年9月 TRANSACTIONS OF THE CHINA WELDING INSTITUTION September 2012

低功率 YAG 激光–TIG 电弧复合焊接镁合金薄板工艺

袁胜涛， 李陈宾， 刘黎明
(大连理工大学 辽宁省先进连接技术重点实验室，大连 116024)

袁胜涛

摘 要： 以2 mm厚AZ31B变形镁合金薄板为研究对象开展低功率脉冲YAG激光–TIG电弧复合热源焊工艺研究，分析了激光与电弧的能量匹配对焊缝成形的影响规律. 结果表明，镁合金薄板低功率YAG激光–TIG电弧复合热源焊接过程中，激光能量与电弧能量之间的相互匹配将直接影响焊缝的表面成形，获得理想焊接接头的工艺参数区间相对较狭小. 为使焊缝成形均匀连续，焊接过程中需要对焊缝背面采用氩气进行保护，当保护气体流量为5～10 L/min时获得了具有最佳性能的焊接接头，其拉伸载荷达到镁合金母材的95%以上.

关键词： 镁合金薄板；激光-TIG电弧复合焊；能量匹配；保护气体流量
中图分类号： TG456.9 **文献标识码：** A **文章编号：** 0253－360X(2012)09－0053－04

0 序 言

镁合金具有质量轻、比强度高、易回收等优点，被誉为“21世纪最有发展前景的绿色工程材料”. 特别是随着节能环保意识的增强，镁合金在汽车制造、航空航天、家电产业等行业中的应用越来越广[1]，因此镁合金及其相关应用技术的研究受到国内外学者的广泛关注. 镁合金的焊接作为镁合金结构件制备的关键环节已经成为现代焊接技术研究的热点之一. 由于镁合金表面张力小、熔沸点低、蒸气压大，焊接过程中金属元素蒸发烧损严重，容易出现表面塌陷、烧穿等缺陷，所以镁合金的焊接对热输入的要求非常严格，特别是镁合金薄板的焊接. 通常情况下采用钨极氩弧焊(TIG)对镁合金薄板进行焊接，由于该方法焊接电流大、速度慢，焊接过程热积累较大，极易出现焊缝成形不连续、塌陷、烧穿等缺陷[2-4]，很难实现镁合金薄板均匀稳定的焊接. 激光焊具有焊接速度高、焊接变形小、热影响区窄、焊缝美观等优点，但是激光焊对工件的装配精度要求较高，容易产生气孔、裂纹、塌陷以及烧穿等缺陷[5].

为了实现镁合金薄板的优质高效焊接，文中提出采用激光－电弧复合热源焊方法对镁合金薄板进行焊接. 研究了低功率YAG激光-TIG电弧复合热源焊接AZ31B镁合金薄板的工艺特点，探讨了激光功率与TIG电弧功率的匹配及背面保护气体流量对缝焊成形的影响规律. 通过调控激光与电弧之间的能量匹配关系，充分发挥了激光与电弧焊各自的优势，为实现镁合金薄板的高速稳定焊接提供了有效的手段.

1 试验方法

采用尺寸为1 000 mm×500 mm×2 mm的变形镁合金AZ31B板材进行对接焊试验. 其化学成分如表1所示. 焊前先用砂纸去除板材表面的氧化膜，再用丙酮清除板材表面的有机物和灰尘并进行干燥处理.

表1 母材的化学成分(质量分数，%)
Table 1 Chemical compositions of base metal

Al	Zn	Si	Mn	Fe	Mg
2.5～3.5	0.5～1.5	0.1	0.2～0.5	≤0.01	余量

采用旁轴式激光-TIG电弧复合焊接方式，其结构示意图如图1所示. 由于镁合金活性较高，易氧化，所以在焊接过程中需要对焊缝及附近高温区域进行保护，试验采用高纯氩气对其进行保护. 焊接时激光在前、电弧在后，TIG焊枪与板材之间的夹角保持在50°. 激光–TIG电弧复合热源焊工艺参数如表2所示.

收稿日期：2012－07－12
基金项目：国家科技重大专项(2009ZX04007-032)

表 2 激光–TIG 电弧复合焊工艺参数

Table 2 Parameters of laser-arc hybrid welding process

激光功率 P_L/W	热源间距 d/mm	TIG 焊接电流 I/A	背面保护气体流量 q/(L·min^{-1})	钨极高度 H/mm	焊接速度 v/(mm·min^{-1})
100 ~ 400	1 ~ 2	70 ~ 120	0 ~ 20	1	1 000 ~ 1 500

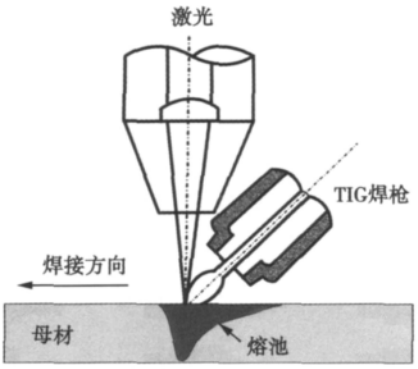

图 1 激光–TIG 电弧复合焊接结构示意图

Fig. 1 Schematic of laser-arc hybrid welding

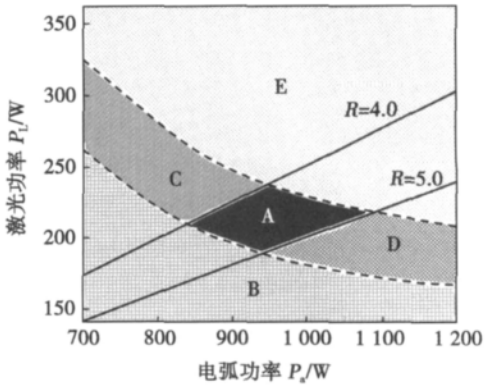

图 2 激光和电弧功率与焊缝成形的关系

Fig. 2 Influence of laser and arc power on formation of welding seam

2 试验结果及分析

2.1 电弧与激光功率匹配对焊缝成形的影响

在薄板镁合金的激光–TIG 电弧复合热源焊接中，受到镁合金自身物理特性的影响，焊缝表面成形不仅取决于激光与电弧热源各自的热输入，同时很大程度上取决于电弧能量与激光能量之间的匹配关系. 特别是在高速焊接条件下电弧受到激光的稳定作用十分显著[6-8]. 试验发现，激光与电弧的整体热输入在高于或低于某一条件时均不能获得理想的焊接接头.

在保证足够的焊接热输入的条件下，电弧功率与激光功率之间存在一个合适的匹配范围. 文中定义电弧热输入与激光热输入之间的比值为 R，其计算方法为

$$R=\frac{P_a/v}{P_L/v}=\frac{P_a}{P_L} \tag{1}$$

式中: P_a 为电弧功率; P_L 为激光功率; v 为焊接速度. 从式(1)中可以看出，电弧与激光热输入的比值即二者功率之间的比值. 通过大量工艺试验，在不同的电弧功率和激光功率匹配下得到了图 2 及图 3 所示的焊缝成形特点分布.

通过对图 2 和图 3 的综合分析，可以发现只有在参数相对较小的区域 A(电弧功率在 850 ~ 1 100 W 之间，R 在 4.0 ~ 5.0 之间)内才能获得较好的焊缝成形. 如图 3a，b 所示，焊缝均匀连续，没有发现塌陷、烧穿等焊接缺陷; 在区域 B 内，当 R 值较大时，

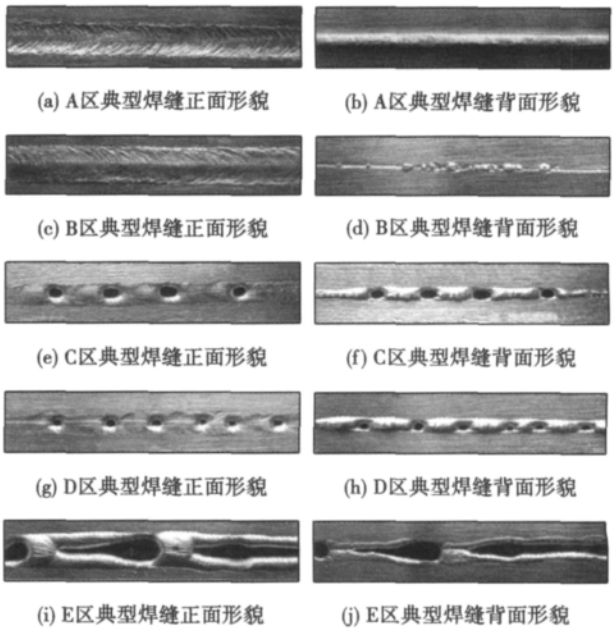

图 3 不同区间典型焊缝形貌

Fig. 3 Typical welding seams at different areas

虽然电弧能量较大，由于激光能量较小，焊接速度较高(1 000 ~ 1 500 mm/min)，不能获得稳定的焊接电弧，当 R 值较小时，电弧能量较小，没有充分发挥出电弧对激光的辅助作用，因此难以实现板材的充分熔化，形成图 3c，d 所示的未焊透的焊接缺陷; 在区域 C 内，焊接电弧功率较小，激光功率相对较大，此时镁合金板材底部的熔合主要依靠激光能量作用，但脉冲激光自身具有不稳定性，易在焊缝局部出现

如图 3e，f 所示的烧穿缺陷；在区域 D 内，由于电弧功率相对较大，电弧热量本身几乎就能使镁合金薄板完全熔化，虽然激光能量相对较小但仍然容易产生连续性烧穿缺陷，如图 3g，h 所示；在区域 E 内，激光功率和电弧功率都较大，造成焊接热输入大，形成宽大的熔池，液态金属表面张力难以维持液态金属的重力，形成图 3i，j 所示连续性烧穿的现象.

综上所述，在镁合金薄板低功率脉冲 YAG 激光-TIG 电弧复合热源对接焊过程中，由于受镁合金自身的物理特性和板材厚度的限制，极易出现各种焊接缺陷，其对激光功率与电弧功率之间的匹配极其敏感，因此焊接过程中能量匹配的精确控制显得尤为重要. 在复合焊接过程中，电弧的加入使激光吸收率大幅的增加导致激光穿透力大大增强，同时激光形成小孔压缩吸引电弧，极大增加了电弧的焊接熔深. 而二者之间所形成热源的稳定性则主要取决于两者之间的匹配关系.

2.2　背面保护气体对焊接成形的影响

试验同时发现，在镁合金薄板激光-TIG 电弧复合焊过程中，由于焊缝背面未使用保护气体，易出现氧化现象进而影响焊接成形[9,10]. 焊缝背面的保护气对镁合金薄板焊接过程整体的稳定性存在着较大的影响. 为进一步探讨背面保护对焊接成形的影响，选取通过能量优化得到的焊接工艺参数（焊接电流 $I=100$ A，激光功率 $P_L=200$ W，焊接速度 $v=1\,400$ mm/min，正面保护气体流量为 10 L/min），对不同的背面保护气体流量作进一步的分析. 背面保护气体流量分别选取 0，5，10，15，20 L/min，不同工艺参数所得结果如图 4 所示.

对图 4 进行分析可以发现，当背面不施加保护气时，由于背面的氧化烧蚀导致焊缝背面局部区域产生瞬间失稳，严重时则会产生烧穿缺陷. 当背面施加流量 5 L/min 和 10 L/min 的保护气体时，一方面可以有效防止背面熔融金属的氧化烧蚀现象，另一方面在一定程度上起到提高冷却速度的作用，进而得到了均匀稳定的背面成形. 当背面保护气体流量增加至 15，20 L/min，此时背面保护气体气压大于焊缝正面气压与熔融金属重力之和，不仅抑制了焊缝熔融金属背面的熔透效果，而且严重时还会使背面焊缝产生内缩现象. 同时背面保护气体不仅会对焊缝表面形貌产生显著的影响，甚至会造成工艺类气孔缺陷. 此类气孔形状不规则，体积一般较大，直径大多高于 0.5 mm，气孔内壁较粗糙，成涡流状，主要在焊缝的中下部位形成（图 4 中当背面保护气体流量为 15 L/min 和 20 L/min 时所得试验现象）.

激光-TIG 电弧复合热源焊接过程中熔池冷却速快，同时镁合金热导率大，导热速度快，因此不会产生毫米级别的氢气孔. 在背面保护气体流量较小时的焊缝中并未发现气孔的存在. 因此这些气孔的形成与背面保护气体流量过大有直接的关系，这主要是由于镁合金在高密度激光的作用下，将迅速熔化、汽化、电离，并在金属蒸气和等离子体压力作用下产生焊接匙孔. 匙孔周围熔化的液体金属在重力和表面张力作用下产生塌陷，导致匙孔根部瞬间失稳，并将匙孔根部的金属蒸气、焊接保护气体及少量侵入匙孔的空气等卷入熔池形成气泡，这类气泡体积一般较大，并且由于镁合金流动性较好，因此少数气泡可以随液体金属流动迁移而逸出熔池. 当镁合金焊接背面保护气体流量较大时，将使得熔池金属的冷却速度加快，部分气泡仍然来不及逸出熔池，即被迅速冷却凝固的金属包围，进而在焊缝中心附近形成气孔.

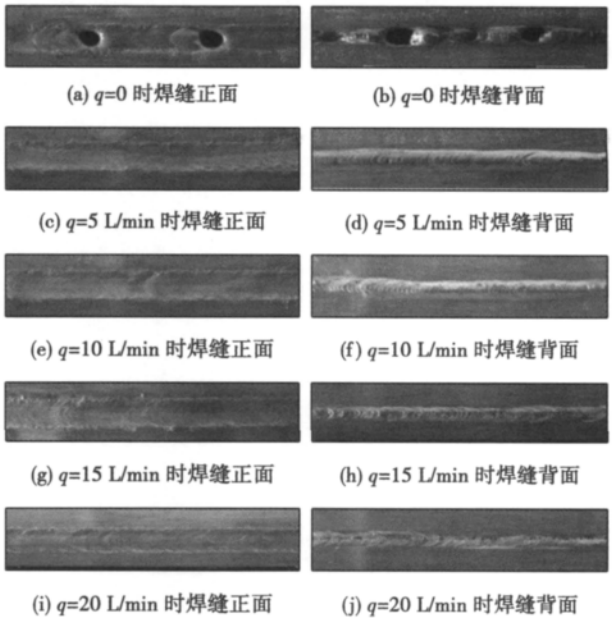

图 4　不同背面保护气体流量下的焊缝形貌

Fig. 4　Welding seams with different flow rates of shielding gas

当背面保护气体略低于或与正面保护气体流量相当时，可以得到良好的焊接头. 焊缝内部气孔率极低. 如图 4 中当背面保护气体流量为 5 L/min 和 10 L/min 时所得焊接结果所示，在这一气体流量范围内，焊后焊缝背面无需打磨即呈现呈淡银白色，具有明显的金属光泽，这说明背面保护效果很好，无金属氧化现象；并且焊缝正面塌陷较小，焊缝背面连续规整成形良好，焊缝内部气孔率极低.

2.3　复合热源焊接接头力学性能

通过上述试验，得到了成形良好的 2 mm 厚

AZ31B 镁合金薄板的激光–TIG 电弧复合焊接头，并对其进行力学性能测试. 测试时按照国家标准 GB2651—89(图 5) 将焊接试件加工成标准试样，采用 Css-2205 形电子万能试验机进行拉伸试验，拉伸速度为 2 mm/min. 拉伸断裂形式如图 6 中所示. 从图 6 中可以看出，拉伸断裂形貌呈 45°斜切面断裂，6 个试样的平均抗拉强度为 220 MPa，其值达到母材强度(230 MPa) 的 95% 以上.

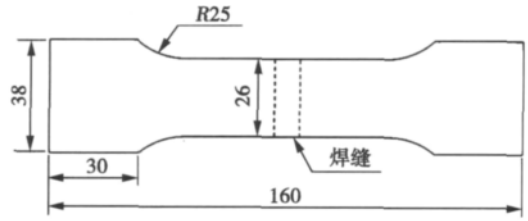

图 5 拉伸试验标准试样(mm)

Fig. 5 Geometry of standard tensile specimens

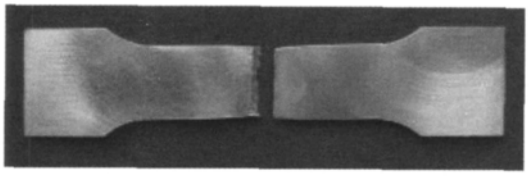

图 6 拉伸断裂宏观形貌

Fig. 6 Macro fracture of specimen in tensile test

3 结 论

(1) 在镁合金薄板低功率 YAG 激光–TIG 电弧复合热源对接焊过程中，焊缝表面成形对热输入较为敏感. 激光功率和 TIG 电弧功率的之间的匹配对于焊缝的成形影响较大，通过调节二者之间的能量匹配可以得到良好的焊缝成形，可以实现复合热源镁合金薄板的优质、高速焊接.

(2) 在复合热源镁合金薄板对接焊过程中添加背面保护气体能够有效的降低焊缝背面的氧化烧蚀. 研究发现，背面保护气体流量为 5 ~ 10 L/min 时，具有最佳的焊接性能，其静态拉伸载荷达到镁合金母材的 95%.

参考文献:

[1] 彭 毅，郑大春. 激光加工在汽车工业生产中的应用 [J]. 新材料新工艺，2000(7)：15 – 17.
Peng Yi，Zheng Dachun. Application of laserprocessing in automobile industry [J]. New Technology and New Process，2000(7)：15 – 17.

[2] 梁国俐，苑少强. AZ31B 镁合金 TIG 焊接工艺研究 [J]. 金属铸锻焊技术，2008(7)：56 – 58.
Liang Guoli，Yuan Shaoqiang. Study on TIG welding technology of AZ31B magnesium alloy [J]. Hot Working Technology，2008(7)：56 – 58.

[3] 全亚杰，陈振华，俞照辉，等. AZ31 镁合金激光焊接头中的缺陷分析 [J]. 热加工工艺，2007，36(3)：33 – 35.
Quan Yajie，Chen Zhenhua，Yu Zhaohui，*et al*. Defects analysis of AZ31 magnesium alloy joints by laser beam welding [J]. Hot Working Technology，2007，36(3)：33 – 35.

[4] 陈祝年. 焊接工程师手册 [M]. 北京：机械工业出版社，2002.

[5] 杨春利，林三宝. 电弧焊基础 [M]. 哈尔滨：哈尔滨工业大学出版社，2003.

[6] 张林杰，张建勋，曹伟杰，等. 工艺参数对 304 不锈钢脉冲 Nd:YAG 激光/TIG 电弧复合焊焊缝成形的影响 [J]. 焊接学报，2011，32(1)：33 – 36.
Zhang Linjie，Zhang Jianxun，Cao Weijie，*et al*. Effects of welding parameters on weld geometry of pulsed Nd:YAG laser/TIG hybrid welding process of 304 stainless steel [J]. Transactions of the China Welding Institution，2011，32(1)：33 – 36.

[7] 李迅波，吴 刚，曾 志，等. 镁合金/不锈钢激光-TIG 复合焊的数值分析 [J]. 焊接学报，2011，32(8)：49 – 52.
Li Xunbo，Wu Gang，Zeng Zhi，*et al*. Numerical analysis of residual stress on magnesium alloy and stainless steel butt joint by hybrid laser-TIG welding [J]. Transactions of the China Welding Institution，2011，32(8)：49 – 52.

[8] Liu Liming，Wang Jifeng，Song Gang. Hybrid laser-TIG welding，laser beam welding and gas tungsten arc welding of AZ31B magnesium alloy [J]. Materials Science and Engineering A，2004，381(1/2)：129 – 133.

[9] Song Gang，Liu Liming. Overlap welding of magnesium AZ31B sheets using laser-arc hybrid process [J]. Materials Science and Engineering A，2006，429(1/2)：312 – 319.

[10] Liu Liming，Hao Xinfeng，Song Gang. A new laser-arc hybrid welding technique based on energy conservation [J]. Materials Transactions，2006，47(6)：1611 – 1614.

作者简介: 袁胜涛，男，1986 年出生，硕士研究生. 主要从事镁合金激光 – 电弧复合热源焊接技术研究. 发表论文 4 篇. Email: gsyuanshengtao@163.com

通讯作者: 刘黎明，男，教授. Email: liulm@dlut.edu.cn

tiation. It was found that the Weibull stress for all specimens is almost identical under the same fracture probability when the interface fracture initiation occurs for different crack-size specimens. Moreover, the interface fracture behavior of one type of specimens with crack can be predicted from the test results of the other type of pre-crack specimens based on the local approach, and the predicted results have a good agreement with the test results. It showed that the local approach not only can be used to describe the interface fracture behavior, but also can be used in the integrity evaluation for interface between different materials.

Key words: coating; interface fracture; local approach; weibull stress

Welding residual stress in T-joint after TIG dressing and its relief LÜ Yishi[1,2], JING Hongyang[1,2], XU Lianyong[1,2], HAN Yongdian[1,2], LIU Faan[3] (1. School of Materials Science and Engineering, Tianjin University, Tianjin 300072, China; 2. Tianjin Key Laboratory of Advanced Joining Technology, Tianjin 300072, China; 3. The Engineering and Design of China Petroleum Group Co., Ltd., North China Branch, Renqiu 062552, China). pp 37 - 40

Abstract: The welding temperature field in T-joint P355NL1 steel plates was measured by using an infrared thermography, and the welding thermal cycle curves were obtained, which have good agreement with the simulation results. The residual stress in T-joint plates was measured by blind-hole method after MAG welding, TIG dressing and heat treatment. The residual stress in T-joint plates was calculated according to the simulated welding temperature field, and the calculated results correspond with the experiment results. The results showed that the method of TIG dressing could lower the residual stress in seam center area to some extent, but the residual stress in remelted area increased. However, the overall heat treatment can effectively relieve residual stress caused by TIG dressing, but there is still partial residual stress in joint.

Key words: TIG dressing; residual stress; overall heat treating; FEM

Analysis on microstructure of particles reinforced Fe-based layers by plasma spray welding LI Lianying, DU Xiaodong, SONG Zili, YE Cheng (School of Materials Science and Engineering, Hefei University of Technology, Hefei 230009, China). pp 41 - 44

Abstract: The WC reinforced Fe-based alloy composite coatings were prepared on the surface of 45 steel by back feeding equipment of plasma spray welding. Scanning electron microscopy (SEM), X-ray diffraction (XRD) and energy diffraction spectrum (EDS) were used to analyze the microstructures and compositions of the coatings. The results show that WC particles are mainly distributed on the top of the coating, and less in the middle and bottom of coating. There are planar crystal, celluler crystal, dendritic crystal and equiaxed crystal from the interface of coating/substrate to the top of the coating. The surface of the coatings has a microstructure consisting of WC, $Fe_{23}B_6$, $Cr_{23}C_6$, Cr_7C_3, SiC, W_2B_5 and FeW_2B_2. The WC particles have dissolution in the spraying process. The dissolution at the top of the coating is higher. The hardness increases from the matrix to the surface of coatings, which is up to 2218 HV.

Key words: plasma spray welding; WC particles reinforced; dissolution; back feeding

Influences of Nd: YAG laser + CMT arc hybrid horizontal welding parameters on weld shape LIU Xiyang[1], WANG Xuyou[1], YUE Yanxing[2], DU Bing[1] (1. Harbin Welding Institute, Harbin 150080, China; 2. Heilongjiang College of Economic Management, Harbin 150040, China). pp 45 - 48

Abstract: The cross-section appearance characteristics of Nd: YAG laser + CMT arc hybrid horizontal welding on 304 stainless steel was evaluated by the welding weld cross-sectional images. The influence of welding parameters on weld cross-section appearance in Nd: YAG laser + CMT arc hybrid horizontal welding were studied. The results indicated that there is a great influence of weld parameters on the weld cross-section shape in YAG laser + CMT arc hybrid horizontal welding. The addition of Nd: YAG laser into CMT arc welding can significantly improve the composite weld and CMT weld penetration in hybrid welded joint. By appropriate welding parameters (the small laser-wire distance, large laser power, the low welding speed, appropriate defocusing distance and low or high CMT power), the mechanical overlay of the weld pool and dislocation of the weld cross-section can be avoided, and the good weld appearance can be obtained.

Key words: laser welding; hybrid horizontal welding; CMT horizontal welding; weld cross-section shape

Mechanism of enhancing effect of electric field on penetration depth of laser-TIG hybrid welding LI Xueyuan, CHEN Minghua, ZHU Meili, LIU Liming (Key Laboratory of Liaoning Advanced Welding and Joining Technology, Dalian University of Technology, Dalian 116024, China). pp 49 - 52

Abstract: The mechanism of the effect of additional electric field on welding penetration depth in laser-TIG hybrid welding was analyzed by comparing with electric field effect on single laser welding and single TIG welding. Meanwhile, the mechanism is verified by the investigation on the effect of electric field at different laser powers and TIG welding currents. Results show that the electric field has influence on the weld penetration depth of laser-TIG welding by controlling the motion of the charges in the plasma in the laser keyhole. The penetration depth can be enhanced when the electrons are forced to move to the bottom of the laser keyhole. The higher laser poweris, the more obvious the enhancing effect of electric fieldis. When the TIG current increases, the effect of electric field is depressed.

Key words: laser-TIG hybrid welding; plasma; electric field; weld penetration

Low power laser-TIG arc hybrid welding of thin magnesium alloy plate YUAN Shengtao, LI Chenbin, LIU Liming (Dalian University of Technology, Key Laboratory of Liaoning Advanced Welding and Joining Technology, Dalian 116024, China). pp 53 - 56

Abstract: Low-power pulsed Nd: YAG laser-TIG hybrid welding process of 2 mm AZ31B magnesium alloy plate was studied. The experiments results showed that the energy cooperation between laser and arc will have influence on the weld appearance

in laser-TIG arc hybrid welding process. The favorable range of hybrid welding parameters was relatively narrow at high welding speed. In order to get the ideal joint, the back of the specimen should be protected by the Ar gas. When the protective gas flow was 5-10 L/min, the favorable performance can be obtained. The tensile strength of laser-arc hybrid welding joint was 95% of Mg base metal.

Key words: magnesium alloy sheet; laser-TIG hybrid welding; power cooperation; shielding gas

Analysis on weld joint performance for matching flux for X100 pipeline steel ZHANG Min[1], ZHANG Xibing[1], CHEN Feichou[1], ZHAO Hongbo[2], BI Zongyue[1,2] (1. School of Materials Science and Engineering, Xi'an University of Technology, Xi'an 710048, China; 2. Baoji Petroleum Steel Pipe Co. Ltd., Baoji 721008, China). pp 57 - 60

Abstract: The uniform design method was used to design the sintering flux for X100 pipeline steel, and five fluorine alkali fluxes with high basicity in couple with welding wire were tested by automatic submerged arc welding. The tensile properties, metallographic structure, hardness value, impact value, impact fracture appearance were analyzed for two kinds of fluxes. The result shows the addition of the appropriate amount of MnO has greater effect on process of flux and toughness of joint. It can improve the weld depth, increase the liquidity of the slag, restrain the undercutting. Meanwhile, it can inhibit the formation of high temperature ferritic structure and be beneficial to the formation of acicular ferrite. In all of five fluxes, the comprehensive performance of No. 2 welded joint is the best, which meets relevant technical standards.

Key words: X100 pipeline steel; automatic submerged arc welding; mechanical properties; metallographic structure

Effect of magnetic field parameters on properties of magnesium alloy welded joint ZONG Lin[1,2], SU Yunhai[2], LIU Zhengjun[2] (1. Shenyang University of Chemical Technology, Shenyang 110870, China; 2. School of Materials Sciences and Engineering, Shenyang University of Technology, Shenyang 110870, China). pp 61 - 64

Abstract: During the welding of AZ31 magnesium alloy plate (5 mm), AC longitudinal and variable frequency magnetic field was used, and the tensile strength and microhardness of welded joint at different magnetic field parameters were tested. With scanning electronic microscope and metallographic microscope, the microstructure of welded joint was analyzed. The effect of magnetic field on the mechanical properties and microstructure of welded joint were studied, and the function mechanism of magnetic field was explored. The results show that the AC longitudinal magnetic field stirs welding pool through the rotating arc, changes the crystallizing process of crystal grains to refine them, which makes the hardness and tensile strength of welded joint improved. Under the proper magnetic field parameter, the electromagnetic stirring achieves the best effect. When magnetic field current $I_c = 2$ A, frequency $f = 20$ Hz, the mechanical properties of welded joint will reach the best value. The hardness is HV 76.2, and the tensile strength is 231 MPa, which is 90% of base metal.

Key words: TIG; longitudinal magnetic field; electromagnetic stirring; magnesium alloy

Nucleation and growth of Cr_7C_3 at interface of brazed diamond with Ni-Cr alloy under protective atmosphere LU Jinbin[1,2], MENG Pu[1], FAN Ping[1], GUO Jian[1] (1. Department of Materials and Chemical Engineering, Zhongyuan University of Technology, Zhengzhou 450007, China; 2. State Key Laboratory of New Type Brazing Alloy and Technology, Zhengzhou Research Institute of Mechanical Engineering, Zhengzhou 450052, China). pp 65 - 68

Abstract: In protective atmosphere furnace, mono-crystalline diamond was brazed with Ni-Cr alloy, the morphology of the carbide formed on the surface of diamond, fracture appearance and microstructures of the brazed seam were analyzed with scanning electron microscope and XRD. The results show that the diamond brazed in protective atmosphere furnace can realize high strength bonding. The brazed diamond has distinct edge and intact morphology. On the surface of the diamond, the arrangement of Cr_3C_2 is regular, the growth directions take on certain orientation relationship with the (111) crystal planes of diamond. All of Cr_7C_3 nucleate and grow on the surface of Cr_3C_2. Finally, the exothecium Cr_7C_3 and regular arrangement endothecium Cr_3C_2 were formed.

Key words: protective atmosphere brazing; diamond; Cr_7C_3; nucleation

Cyclical behavior of lead-free BGA soldered joints based on nano-indentation method LIU Meina, WANG Lifeng, LÜ Ye, DAI Hongbin, YANG Wenxuan (College of Materials Science and Engineering, Harbin University of Science and Technology, Harbin 150040, China). pp 69 - 72

Abstract: Through the cycle loading test of nano-indentation method, the effects of maximum load, cycle number and holding time for two kinds BGA soldered joints of Sn-3.0Ag-0.5Cu and Sn-0.3Ag-0.7Cu on cycling performance were investigated. The results indicated that the cycling performance of Sn-Ag-Cu series lead-free BGA soldered joints was load-dependent, and the cumulative damage of BGA soldered joints increased with the increasing of maximum load, especially largely accumulated in the first few cycles, then gradually decreased and stabilized. However, with the cycle number increasing, the deformation resistance of BGA soldered joints slightly decreased; the creep displacement increased with the holding time being increased and the creep-fatigue interaction will accelerate the failure of BGA soldered joints. The energy loss of Sn-0.3Ag-0.7Cu BGA soldered joints is greater than that of the Sn-3.0Ag-0.5Cu BGA solder joints.

Key words: lead-free solder; cycle load-unload; nano-indentation method; creep

Development of slag-free self-shielded flux cored wire with niobium addition for hardfacing LIU Dashuang, LIU Renpei, QIU Yue, GAO Wenliang (College of Material Science and Technology, Nanjing University of Aeronautics and Astronautics,